RSC Advances

REVIEW

View Article Online
View Journal | View Issue

Cite this: *RSC Adv.*, 2026, **16**, 25116

Engineering $Ti_3C_2T_x$ (titanium carbide) MXene-based composites and emerging applications: a mini review

Ly Tan Nhiem *

Two-dimensional $Ti_3C_2T_x$ MXene has attracted considerable attention owing to its metallic conductivity, tunable surface terminations, and structural versatility, which underpin its broad functional applicability. Although numerous review articles have addressed $Ti_3C_2T_x$ MXene-based composites, most have primarily focused on energy storage and energy conversion systems. In contrast, this review provides a fundamental and up-to-date overview of $Ti_3C_2T_x$ MXene research in recent years, emphasizing the relationship between synthesis strategies, surface termination control, structural and electronic properties, and application-specific performance. First, various synthesis routes are discussed with particular emphasis on how etching conditions, post-treatment processes, and delamination strategies regulate the surface termination groups (–O, –OH, and –F) and defect structures of $Ti_3C_2T_x$. These surface chemistries critically influence the electronic structure, interlayer spacing, hydrophilicity, and charge transport characteristics of the material. Subsequently, the resulting structure–property relationships are analyzed to explain how these physicochemical features govern functional performance in different technological applications. Particular attention is devoted to integrating experimental observations with density functional theory (DFT) calculations to elucidate reaction mechanisms and interfacial interactions. Finally, applications in sensing, energy harvesting, water splitting, water remediation, and biomedical technologies are systematically discussed. By correlating synthesis parameters with surface chemistry and electronic structure, this review aims to provide a fundamental framework for understanding current challenges and guiding the rational design and scalable deployment of $Ti_3C_2T_x$ MXene-based systems.

Received 4th November 2025
Accepted 23rd April 2026

DOI: 10.1039/d5ra08486e

rsc.li/rsc-advances

Introduction

Nowadays, nanoscience and engineering, particularly of two-dimensional (2D) nanomaterials, have become a central focus of both fundamental research and industrial commercialization due to their unique physicochemical properties.[1–5] Among them, the exploration of 2D $Ti_3C_2T_x$ in the year of 2011 introduced a novel class of 2D materials known as MXene.[6,7] MXene possesses diverse elemental compositions, natural hydrophilicity, unique 2D structures with multilayered shapes, large surface areas with abundant surface termination groups, good conductivity, and excellent optoelectronic properties.[8,9] To date, more than 35 stoichiometric phases have been identified with hexagonal P_{63}/mmc symmetry. MXene sandwiched layers are produced by removing A layers from the MAX phase precursor (A represents Ga, Si, Al, *etc.*).[10] There are several methods to break the chemically bonded A layer in MAX phases, such as top–down synthesis techniques and wet chemical etching.[11] These methods can be summarized into several categories, including alkaline hydrothermal treatments, hydrofluoric acid (HF) and HF-containing etchant treatment, HF-forming etchant treatment, and molten-salt etching methods.

In general, the MXene class of materials is composed of transition metal carbides, nitrides, and carbonitrides, with the general formula $M_{n+1}X_nT_x$ (n = 1, 2, or 3), where M, X, and T_x represent a transition metal, N and/or C atoms, and surface termination groups, respectively.[10,12,13] MXenes with $n > 3$ were only explored as minor impurity phases or in radiofrequency sputtered thin films.[6] Recently, Deysher and co-workers successfully synthesized an $(Mo_{0.8}V_{0.2})_5AlC_4$ MAX phase with the molar ratio of Mo : V : V_2O_3 : Al : C of ~4 : 0.9 : 0.05 : 1.2 : 3.5 under an Ar flow *via* a powder metallurgy technique. Then, $(Mo_{0.8}V_{0.2})C_4T_x$ was also etched using HF acid at 50 °C in an oil bath for 8 days.[14] It is important to note that HF was utilized for etching Al layers, thereby creating additional space for electrochemical Li intercalation in battery research.[15] The etching conditions were tuned to optimize the yields and minimize the destruction of the MXene nanosheets in liquid acid.[16] The surface termination groups of the Ti_3AlC_2 MXene depend on the etching conditions. When HF acid was used for etching, F

Faculty of Chemical and Food Technology, Ho Chi Minh City University of Technology and Engineering, 01 Vo Van Ngan Street, Thu Duc Ward, Ho Chi Minh City, Vietnam. E-mail: nhiemlt@hcmute.edu.vn

terminations dominate, while when molten chloride salts were used, Cl-rich surfaces are obtained.[17]

In addition, as synthesis routes and surface terminations critically influence reproducibility, scalability, and application-specific performance, it is necessary not only to select high-quality MAX phases and precisely control the synthesis strategy, including appropriate etchants and dosages, but also to employ encapsulation strategies, construct MXene-derived composites, or utilize suitable surfactants to stabilize MXenes. One of the main drawbacks of MXene materials is their high susceptibility to oxidation under environmental conditions such as elevated temperature, high humidity, and exposure to air or oxygen (1–2 months). In particular, structural degradation of $Ti_3C_2T_x$ can occur even in the absence of external oxidizing agents at elevated temperatures, which is attributed to the interaction between molecular hydrogen and surface functional groups trapped between the interlayers. It has been reported that oxidation preferentially occurs at defective sites or –OH/–O-terminated sites rather than at –F-terminated sites, owing to the diffusion of Ti^{4+} and O^{2-} ions, which participate in the oxidation process. Thermal heat treatment and storing samples under refrigerated or deoxygenated conditions are considered effective strategies to mitigate the oxidation of $Ti_3C_2T_x$ nanostructures. Moreover, representative stabilizing agents include 1H,1H,2H,2H-perfluoroalkylsilane, sodium L-ascorbate, sodium dodecyl sulfate, and (3-chloropropyl) trimethoxysilane.[18,19] It is essential to recognize and address the long-term stability issues of MXenes during storage and utilization, as they are strongly influenced by the preparation methods employed. Under humid or elevated-temperature conditions, MXenes are prone to degradation and oxidation into TiO_2 and amorphous C, which significantly restricts their large-scale commercialization and practical applications. On the one hand, current storage strategies, such as dispersing MXenes in organic solvents, storing them at low or cryogenic temperatures, or sealing them under inert atmospheres, can effectively extend their storage lifetime. However, these approaches primarily delay degradation rather than fundamentally preventing it. On the other hand, more intrinsic stabilization strategies have been proposed, including minimizing defect sites on MXene surfaces and edges through surface functionalization, edge or surface passivation, encapsulation, and hydrogen-based thermal treatments.[20] These approaches aim to directly suppress oxidation pathways and offer more sustainable solutions for improving the durability of MXenes.

As mentioned previously, owing to the surface functional groups (typically –Cl, –F, =O, and –OH), $Ti_3C_2T_x$ MXenes have excellent properties such as hydrophilicity, desirable optical, scalability, mechanical and electrical properties.[6,21] Since their discovery, $Ti_3C_2T_x$ MXenes have attracted increasing research interest thanks to their broad range of applications in energy storage, gas and pressure sensors, and electromagnetic interference shielding, depending on their surface termination groups and compositions.[22] Different from their parent MAX phases, $Ti_3C_2T_x$ MXenes can be easily intercalated between layers using sonication and polar organic solvents such as dimethyl sulfoxide (DMSO), tetrabutylammonium hydroxide (TBAOH), and *n*-butylamine.[23] $Ti_3C_2T_x$ MXene materials can be well dispersed in liquids without any surfactant thanks to their hydrophilicity. Following this, $Ti_3C_2T_x$ MXene's properties can be enhanced by forming composites with metal oxide semiconductors.[24] There are many reports predicting the properties of these types of heterostructures and their potential applications, thereby expanding opportunities for the scientific community.[25]

In recent years, numerous review articles have summarized MXene-based materials, with a predominant focus on energy-related applications such as supercapacitors, batteries, and electrocatalysis.[26–29] However, rapid developments in synthesis strategies, surface functionalization, and emerging multifunctional applications have not been updated or compared across different research directions. In particular, the integration of experimental observations with theoretical studies, such as DFT calculations, remains underrepresented in existing reviews, despite its importance for understanding structure–property relationships and guiding rational material design. Moreover, DFT calculations can be used to predict composite configurations, estimate electrocatalytic reaction performance, and elucidate the relationships between material composition, properties, and performance, thereby providing guidance for material synthesis as well as a better understanding of plausible reaction mechanisms.[26]

This review aims to provide a focused and updated perspective on metallic $Ti_3C_2T_x$ MXene research by critically analyzing recent progress reported primarily over the past five years. Unlike many existing reviews that predominantly emphasize energy storage and electrochemical applications, this work highlights the broader multifunctionality of $Ti_3C_2T_x$ MXenes, including emerging roles in photonics, sensing, catalysis, and environmental technologies. To clearly distinguish this review from the prior literature, we adopt a structure–property–performance framework that systematically links synthesis strategies and surface termination engineering with the resulting electronic and physicochemical properties governing application-specific performance. In addition, this review incorporates technological readiness levels (TRLs), cost considerations, and realistic commercialization perspectives, supported by recent global MXene market forecasts (*e.g.*, MXene Market Insights, with projections up to 2033). A comparative overview of representative 2D materials (MXenes, borophene, and graphene) is also provided to highlight their respective properties, strengths, and limitations. Furthermore, the selected studies emphasize advances in surface chemistry control, scalable synthesis approaches, and performance mechanisms validated through both experimental investigations and theoretical calculations, including density functional theory (DFT). By integrating experimental observations with theoretical understanding, this review aims to clarify key design principles for $Ti_3C_2T_x$-based composites and highlight opportunities for scalable production and practical implementation. Finally, we discuss current limitations and future research directions that may accelerate the industrial translation of $Ti_3C_2T_x$ MXene technologies.

Synthesis and properties of $Ti_3C_2T_x$ MXenes

Although MXene synthesis is often associated with HF, fluorine-containing compounds are well known for their severe toxicity and hazardous effects, including potential impacts on the nervous, skeletal, and reproductive systems, as well as dental health. However, despite these risks, relatively few studies have quantitatively examined fluorine-related safety issues and laboratory accidents during MXene synthesis, which remain a significant bottleneck for their large-scale commercialization. According to a clinical report, the serum calcium level of a patient exposed to HF acid was approximately 4.9 mg dL^{-1}, which is substantially lower than the normal physiological range of 8.4–10.2 mg dL^{-1}.[27] Therefore, strict safety protocols and emergency response guidelines are essential when handling fluorine-containing aqueous solutions, regardless of their concentration, and appropriate laboratory protective equipment must always be employed.

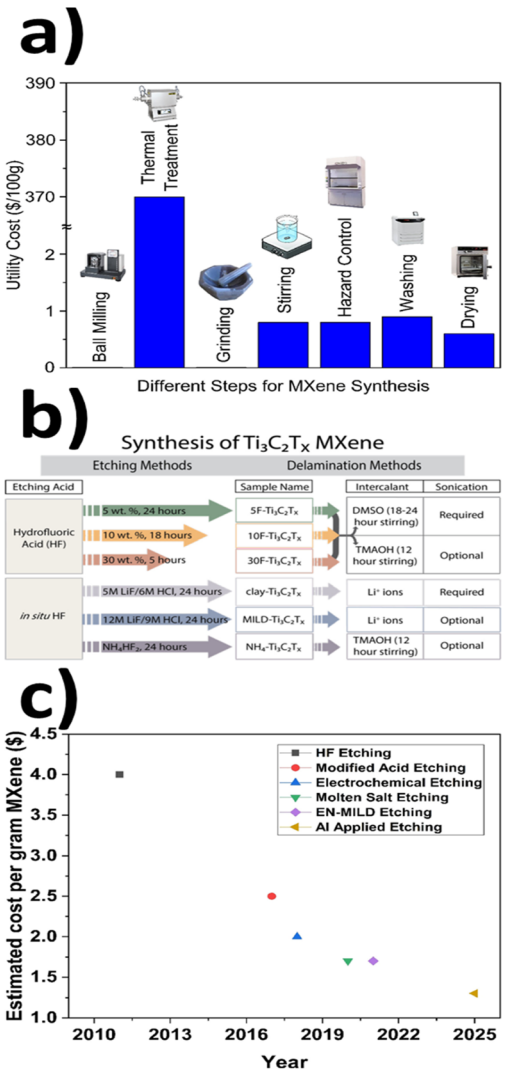

Fig. 1 Schematic of (a and c) cost consideration, adapted/reproduced from ref. 22 with permission from Elsevier, Copyright 2026. (b) General method for $Ti_3C_2T_x$ MXene synthesis from Ti_3AlC_2 MAX phase, adapted/reproduced from ref. 35 with permission from the American Chemical Society, Copyright 2017.

Fluoride-based methods

$Ti_3C_2T_x$ MXenes are synthesized *via* the wet chemical technique from Ti_3AlC_2 MAX phases in HF solution or *via in situ* HF generation using a mixture of LiF and HCl as well as NH_4HF_2, as shown in Fig. 1.[30,31] In particular, typically F-containing etchants are utilized to selectively eliminate the Al layer, releasing termination groups T_x. These methods are easy to perform; however, the acute toxicity of fluoride-containing acidic solutions poses a challenge in aqueous processing and hinders scale-up. Moreover, the wastewater after the experiment should be treated well before its release into the natural environment. Each technique has its own pros as well as cons, which can be briefly expressed through the following chemical reactions for Ti_3AlC_2:[32]

$$Ti_3AlC_2 + 3HF \rightarrow AlF_3 + 3/2H_2 + Ti_3C_2T_x \quad (1.1)$$

$$Ti_3C_2T_x + 2HF \rightarrow Ti_3C_2F_2 + H_2 \quad (1.2)$$

$$Ti_3C_2T_x + 2H_2O \rightarrow Ti_3C_2(OH)_2 + H_2 \quad (1.3)$$

The quality of $Ti_3C_2T_x$ MXenes depends not only on the choice of etchant, synthesis scale, and molar ratios, but also on the external forces applied during delamination and post-treatment processes. For instance, sonication-assisted delamination typically yields small-sized flakes (~200–500 nm), whereas manual shaking produces significantly larger flakes, with lateral sizes ranging from ~4 to 15 μm.[33] Furthermore, centrifugation speed strongly influences size selection: at 5000 rpm, the collected MXene supernatant predominantly contains small flakes with an average size of 0.11 ± 0.07 μm, while centrifugation at 1000 rpm yields larger flakes with an average size of 0.8 ± 0.3 μm.[34]

Halogen etching of Ti_3AlC_2 MAX phase

In 2021, a new method to etch the Ti_3AlC_2 MAX phase was explored by Richard and colleagues using elemental halogens, as shown in Fig. 2a. In this study, the aluminum halide was generated during the etching process, along with halogenated $Ti_3C_2T_x$ with 1% yield MXene (at 1 mg mL^{-1}). The $Ti_3C_2T_x$ crude was decontaminated by washing with a nonpolar solvent ($CHCl_3$) several times.[36] As shown in Fig. 2b, the plasmonic resonance exhibits a gradual red shift across different surface terminations, which may correlate with variations in the electronegativity of the functional groups (F > Cl > Br > I) and the resulting polarization of the Ti–halogen bonds. Although electron density redistribution is likely involved, the underlying mechanisms governing the observed plasmonic trends remain insufficiently clarified and warrant further systematic experimental and theoretical investigations.

These approaches remain largely academic due to significant challenges related to cost, safety, scalability, and

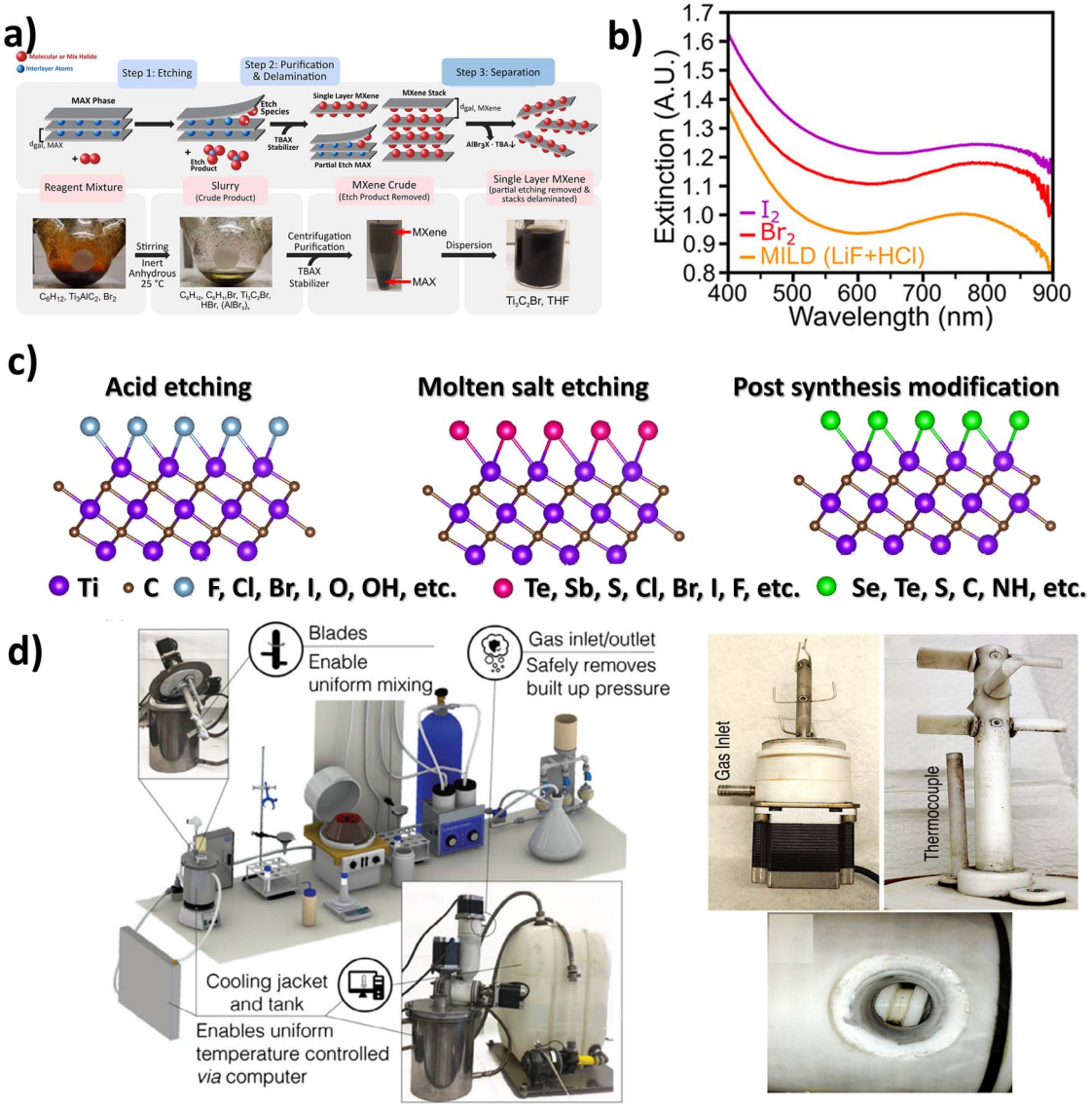

Fig. 2 (a) Schematic of the halogen etching of Ti_3AlC_2 MAX phase and (b) extinction spectra of conventional $Ti_3C_2T_x$ MXene and halogen-terminated $Ti_3C_2T_x$ MXenes synthesized *via* different etching routes, adapted/reproduced from ref. 36 with permission from the American Chemical Society, Copyright 2021. (c) Highlighting the dependence of surface functional groups on the synthesis technique, adapted/reproduced from ref. 37 with permission from Elsevier, Copyright 2025. (d) Photograph of the 1 L batch MXene synthesis system integrated with a cooling tank, adapted/reproduced from ref. 32 with permission from John Wiley and Sons, Copyright 2020.

reproducibility. Beyond the highly reactive and toxic nature of halogen species, a major limitation is that the entire process must be conducted under an inert atmosphere within an isolated glovebox. Moreover, Br_2 poses severe corrosion risks to metallic parts of glovebox systems, resulting in unacceptable operational hazards. In addition, the treatment of halogenated waste and the continuous consumption of inert gases further increase operational costs and safety concerns.

Despite significant achievements in the synthesis of $Ti_3C_2T_x$ MXenes, scaling up their production remains a major challenge that limits their large-scale industrial deployment. Over the past 15 years, several advanced etching strategies have been developed. Among them, *in situ* HF generation *via* the minimally intensive layer delamination (MILD) method has been widely adopted due to its relatively simple implementation, high yield, and improved flake quality compared to direct HF etching. However, this approach still generates corrosive wastewater and may lead to surface termination heterogeneity and structural inconsistencies. In contrast, fluoride-free alkaline etching strategies, which aim to synthesize $Ti_3C_2T_x$ MXenes without fluorine terminations, offer enhanced control over surface chemistry and intrinsic properties while reducing fluorine-related environmental and safety concerns; nevertheless, these methods often require stringent reaction conditions and currently suffer from limited etching efficiency and material yield. Molten salt synthesis represents another promising route that meets basic requirements for MXene formation and enables the production of fluorine-free or termination-tunable

Table 1 Comparative benchmarking of $Ti_3C_2T_x$ MXene etching strategies

Synthesis method	Typical yield	Flake size	Electrical conductivity	Defect density	Oxidation stability	Cost	Environmental burden	Scalability
HF etching	High (>80%)	Large (5–20 μm)	Moderate (5000–10 000 S cm^{-1})	Moderate	Low–moderate	Low	High (toxic HF)	Good (lab–pilot)
Mild (LiF/HCl)	High	Large (5–25 μm)	High (10 000–15 000 S cm^{-1})	Low–moderate	Moderate	Moderate	Medium	Excellent
F-free etching	Moderate	Medium (1–10 μm)	Moderate	Moderate–high	Moderate	Moderate–high	Low	Developing
Halogen etching	Moderate	Small–medium	High (low –F terminations)	Low	High	High	High (corrosive gases)	Limited
Molten salt etching	Moderate–high	Small–medium	High (low defect, –Cl terminations)	Low	High	Moderate–high	Medium	Promising (industrial potential)

MXenes (Fig. 2c); however, its practical application is constrained by high operating temperatures, significant energy consumption, and complex post-treatment processes.

According to the list of precursors required for Ti_3AlC_2 MAX phase preparation and their corresponding prices from Merck, the estimated cost of the raw precursors for Ti_3AlC_2 is approximately USD 421 per 100 g, excluding processing, manufacturing, and other associated variables (Table S1). Overall, each conventional synthesis technique presents inherent advantages and drawbacks, including issues related to energy consumption, hazardous byproducts, equipment complexity, and safety concerns. Therefore, the development of green, scalable, and sustainable synthesis strategies is critically important to align $Ti_3C_2T_x$ MXene production with sustainable development goals and to enable large-scale commercialization for diverse applications (Table 1).

An overview of the techno-economic analysis of $Ti_3C_2T_x$ is essential, as this material has attracted significant attention in recent years, accompanied by continuous efforts to develop novel preparation methods, enhance scalability, and promote commercialization and industrial applications that were not comprehensively addressed in earlier assessments. Wet chemical etching routes appear to remain the most cost-effective at the laboratory scale due to their relatively low energy consumption and high yield. However, their industrial translation is constrained by hazardous waste management requirements and regulatory compliance costs. In contrast, fluoride-free and molten-salt strategies reduce environmental burdens but introduce higher energy demands and greater process complexity. In fact, no single synthesis route currently satisfies all sustainability criteria (Table S2). Therefore, efforts should focus on balancing chemical intensity, energy input, operational safety, and product quality through systematic process optimization and green engineering approaches.

Properties of metallic $Ti_3C_2T_x$ MXene

It is well-known that $Ti_3C_2T_x$ MXenes have excellent electrical conductivity (11 000 S cm^{-1}; monolayer $Ti_3C_2T_x$ MXene) compared with $Ti_3C_2T_x$ flakes (4600 S cm^{-1}) due to the d–d orbitals of the Ti atom and rich T_x surface functional groups in $Ti_3C_2T_x$ MXenes. These electrical properties could help $Ti_3C_2T_x$ MXene become a good candidate for applications in the fields of energy storage, gas sensing, and EMI shielding.[38] Besides, owing to the strong quantum confinement of $Ti_3C_2T_x$ MXene quantum dots (MQDs) with an average size of around 3–6 nm, they exhibited excitation-dependent PL with high quantum yields (10%). $Ti_3C_2T_x$ MQDs displayed excellent solubility in both ethanol and DI water due to the strong hydrophilic properties.[39] As shown in Fig. 3, MXene-based films could be deformed in various shapes, such as membranes, stamping, and a paper airplane. It is important to know that pure $Ti_3C_2T_x$ MXenes with a 3D macroporous architecture exhibit superior flexibility and strong moldability.[40] Moreover, the electrochemical properties of $Ti_3C_2T_x$ MXenes in a flexible micro-supercapacitor toward wearable flexible electronics were investigated under bending during operation.[41] In particular, $Ti_3C_2T_x$

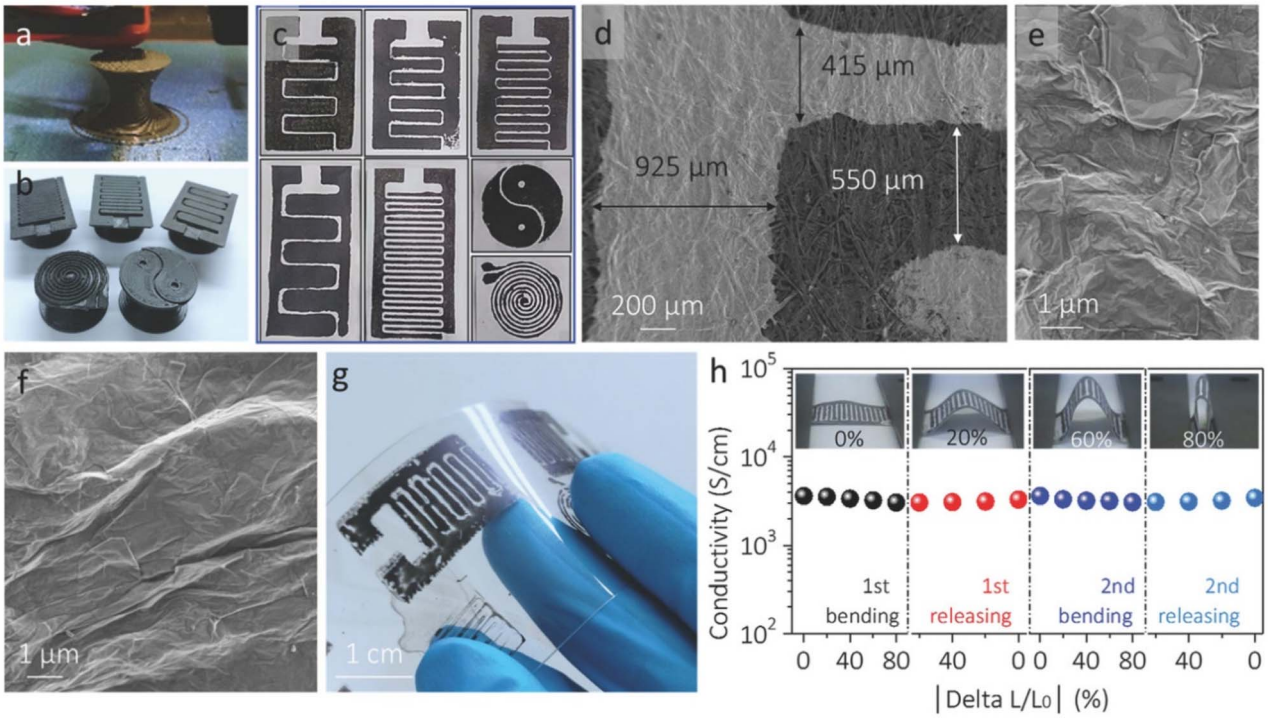

Fig. 3 (a–c and g) Photographs of stamped MXene microsupercapacitors with different device architectures. (d–f) SEM images of the interdigitated electrodes on the corresponding substrates. (h) Photographs of the device under four different bending states and the corresponding resistance changes, adapted/reproduced from ref. 53 with permission from John Wiley and Sons, Copyright 2018.

MXenes are not stable in the natural environment for long times. The oxidation process was accelerated in the presence of dissolved oxygen, exclusively in water. $Ti_3C_2T_x$ MXenes can be degraded into TiO_2 and methane after a long time of storage, which poses a challenge to the research community. They should be kept in a refrigerator or an inert environment at low temperatures.[42]

DFT calculations indicate that the work function of metallic MXene is approximately −5.35 eV, which decreases to −6.88 eV after a light oxidation process. The HOMO and LUMO levels are located at approximately −7.23 eV and −3.26 eV, respectively. The DFT-based calculations of the energy levels of MXenes after their oxidation confirm that they exhibit semiconducting behavior.[26]

Tables 2 and S3 summarize the physical and chemical properties of MXenes, which are compared with those of other representative 2D materials. Although several experimental techniques are available to characterize the structure, morphology, and composition of materials, these methods are often time-consuming and costly. Therefore, theoretical calculations are expected to provide efficient and accurate analyses that support a deeper understanding of the physicochemical

Table 2 Physicochemical properties of $Ti_3C_2T_x$ MXenes

Category	Property	Typical values
Chemical stability	pH stability	Stable in mild acidic/neutral media[43]
	Oxidation sensitivity	Degrades in O_2, light, high humidity[44]
Adsorption properties	Surface area	~10–100 $m^2\ g^{-1}$ (ref. 45)
	Adsorption sites	Ti–O, Ti–OH, defects[46]
Chemical properties	Hydrophilicity	Strongly hydrophilic[47]
	Chemical reactivity	Easily oxidized (TiO_2 formed in air/water)[48]
	Redox activity	Ti^{4+}/Ti^{3+} surface states[49]
Mechanical properties	Young's modulus	~330 GPa (monolayer, theoretical)[50]
	Flexibility	High (bendable films)[50]
Thermal properties	Thermal conductivity	~10–100 $W\ m^{-1}\ K^{-1}$ (ref. 51)
Electronic properties	Conductivity	~10^3–10^4 $S\ cm^{-1}$ (ref. 52)
	Band structure	Metallic to semi-metallic[52]
	Work function	~4.6–5.2 eV (T_x dependent)[52]
Surface chemistry	Terminal groups	–O, –OH, –F, –Cl, –Br, –I…[37]
	Surface charge	Negative zeta potential (−35 mV)[43]

properties of MXenes and their derivatives, particularly with respect to interfacial properties and relative stability.

A recent study by Mostafa's group evaluated the environmental impacts and cumulative energy demand associated with MXene synthesis from gram- to kilogram-scale production. Their results indicate that more than 70% of the total environmental impact arises from electricity consumption. At the laboratory scale, the production of 1000 g of MXene releases approximately 428.1 kg of CO_2, whereas the industrial-scale manufacture of 1 kg of copper foil results in only ~8.75 kg of CO_2 emissions.[54] This substantial discrepancy is primarily attributed to intensive chemical consumption and the associated wastewater treatment processes. To mitigate these impacts, the authors proposed synthesizing secondary MXenes from MAX phases derived from secondary precursors, such as tire-recycled carbon, aluminum scrap, and titanium dioxide. Notably, the resulting secondary MXenes exhibit competitive electrical conductivity (5857 ± 680 S cm^{-1}), comparable to that of conventionally synthesized MXenes.[55] Furthermore, the integration of artificial intelligence and computational modeling is expected to play a critical role in optimizing synthesis parameters for secondary MXenes. The millions of tons of titanium and aluminum scrap worldwide offer promising precursors and a pathway toward the scalable, low-cost, and sustainable production of high-quality MXenes.

Applications of $Ti_3C_2T_x$ MXenes and $Ti_3C_2T_x$ MXene-based composites

Scientists worldwide have increasingly focused on the development of multifunctional materials capable of delivering high performance across diverse application domains. In this context, $Ti_3C_2T_x$ MXene-based nanocomposites have emerged as a potential material platform due to their unique properties. These attributes enable their effective deployment in strategic applications, including energy storage and conversion, gas sensing, and water splitting, which are closely linked to national energy security and technological competitiveness. Simultaneously, $Ti_3C_2T_x$ MXene nanocomposites offer substantial benefits for societal applications, such as soft tissue regeneration and environmental remediation, addressing pressing challenges related to sustainability, public health, and environmental protection. Therefore, systematic investigation of $Ti_3C_2T_x$ MXenes and their nanocomposites is crucial to fully exploit their multifunctionality and to bridge strategic technological advancement with societal needs.

$Ti_3C_2T_x$ based platforms for soft tissue regeneration

The versatility of $Ti_3C_2T_x$ nanostructures allows for their composites to be multifunctional systems, especially in bone tissue regeneration and engineering.[56,57] For example, $Ti_3C_2T_x$-based platforms can be combined with biomaterials to construct composite scaffolds with tailored functionalities and improved mechanical behaviors. These optimized nanostructures offer synergistic effects, integrating the strength of each compound to provide specific tissue regeneration demands.[58–60] $Ti_3C_2T_x$-based composites can also be integrated

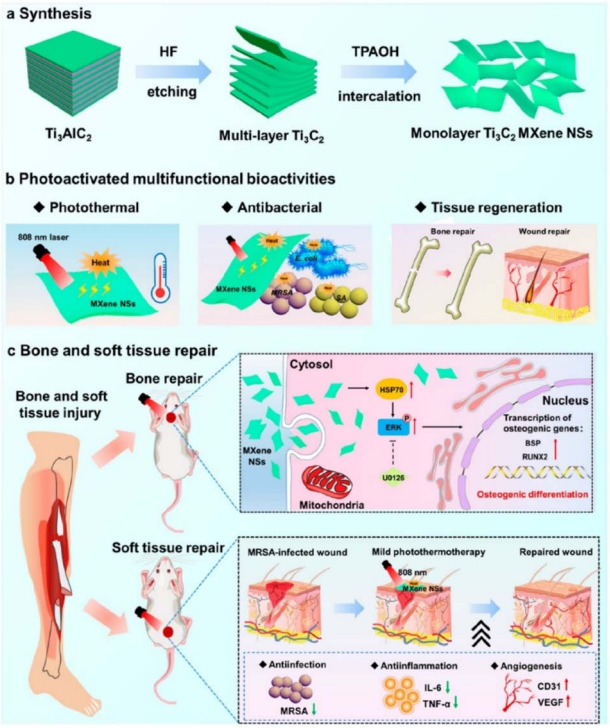

Fig. 4 (a) Synthesis procedure, (b) multifunctional bioactivities, and (c) photoactivated $Ti_3C_2T_x$ nanostructures for biomedical applications, adapted/reproduced from ref. 62 with permission from the American Chemical Society, Copyright 2023.

with drug delivery systems, improving the controlled release of therapeutics to enhance tissue regeneration results.

Although $Ti_3C_2T_x$ nanostructures have many unique properties and inherent hydrophilic behavior,[61] tailoring these properties to suit the specific demands of bone and soft tissue regeneration is a challenging and sophisticated goal. It is important to fully understand the fundamentals of the structural properties of $Ti_3C_2T_x$ MXenes and how to control their operational parameters. In other words, the integrated bone-soft tissue regeneration facilitated by $Ti_3C_2T_x$ MXenes offers several advantages, such as improved healing, reduced risk of infection, and targeted drug delivery. The integrated thermal effects of photoactivated $Ti_3C_2T_x$ MXenes have been shown to enhance tissue regeneration, providing a potential technique for tissue repair. As shown in Fig. 4, Xiaoyan and co-workers have demonstrated that a photoactivated $Ti_3C_2T_x$ MXene exerts positive effects on the improvement of soft and bone tissue regeneration. The photoactivated $Ti_3C_2T_x$ MXene displayed not only a strong thermal effect but also a robust antibacterial performance, effectively modulating the expression of inflammation factors (methicillin-resistant *Staphylococcus aureus*).[62] Moreover, this technique enables the regulation of the osteogenic differentiation of adipose-derived stem cells through heat shock protein 70 and an extracellular signal-regulated kinase signaling pathway. However, despite these good outcomes, their study has some limitations. On the one hand, scale-up of high-quality $Ti_3C_2T_x$ nanostructures remains

Table 3 Representative $Ti_3C_2T_x$ MXene-based platforms for biomedical applications

$Ti_3C_2T_x$-based platform	Applications and representative functions	Main advantages	Ref.
$Ti_3C_2T_x$ MXene	- Skin wound healing	- Good cytocompatibility and photothermal conversion	67 and 68
	- Accelerated wound closure; infection suppression	- High antibacterial activity	
$Ti_3C_2T_x$-incorporated hydrogel	- Skin and soft tissue repair - Promotes angiogenesis and tissue remodeling	- Injectable and flexible - Enhanced cell adhesion and proliferation	69 and 70
$Ti_3C_2T_x$-polymer composite	- Tissue engineering - Enhances fibroblast migration and epithelialization	- High electrical conductivity - Mechanical robustness - Moisture retention	71 and 72
$Ti_3C_2T_x$-poly(lactic acid)	- Bone tissue regeneration and engineering	- Optimization NO release - High photothermal effects - Suitable tensile strength	73
$Ti_3C_2T_x$-PLCL/collagen	- Spontaneous osteogenic differentiation. Bone tissue regeneration and engineering	- The growth of preosteoblasts - NIR photon absorption - High biocompatibility stability	74

a challenge for the science community.[63] Also, another difficulty is controlling the surface termination groups (–OH, –O, and –Cl) and preventing their rapid accumulation in biological media.[64] On the other hand, long-term storage of non-oxidized $Ti_3C_2T_x$ nanosheets is difficult to control,[65,66] and the toxicological investigation of $Ti_3C_2T_x$ nanostructures *in vivo* must be performed systematically.

Based on the reported achievements of MXene-based composites in soft and bone tissue regeneration (Table 3), several key research directions remain to be addressed to further enhance osteogenic differentiation and cell adhesion within scaffolds. These include (i) mimicking the native bone architecture to provide appropriate structural and biochemical cues; (ii) improving mechanical properties to better match those of natural bone; (iii) enhancing osteoinductive capacity to promote stem cell differentiation; (iv) facilitating vascularization and efficient nutrient and waste transport; (v) ensuring long-term stability and seamless integration with host tissue; (vi) achieving scalable and cost-effective fabrication; and (vii) advancing clinical translation through standardized evaluation and regulatory approval.

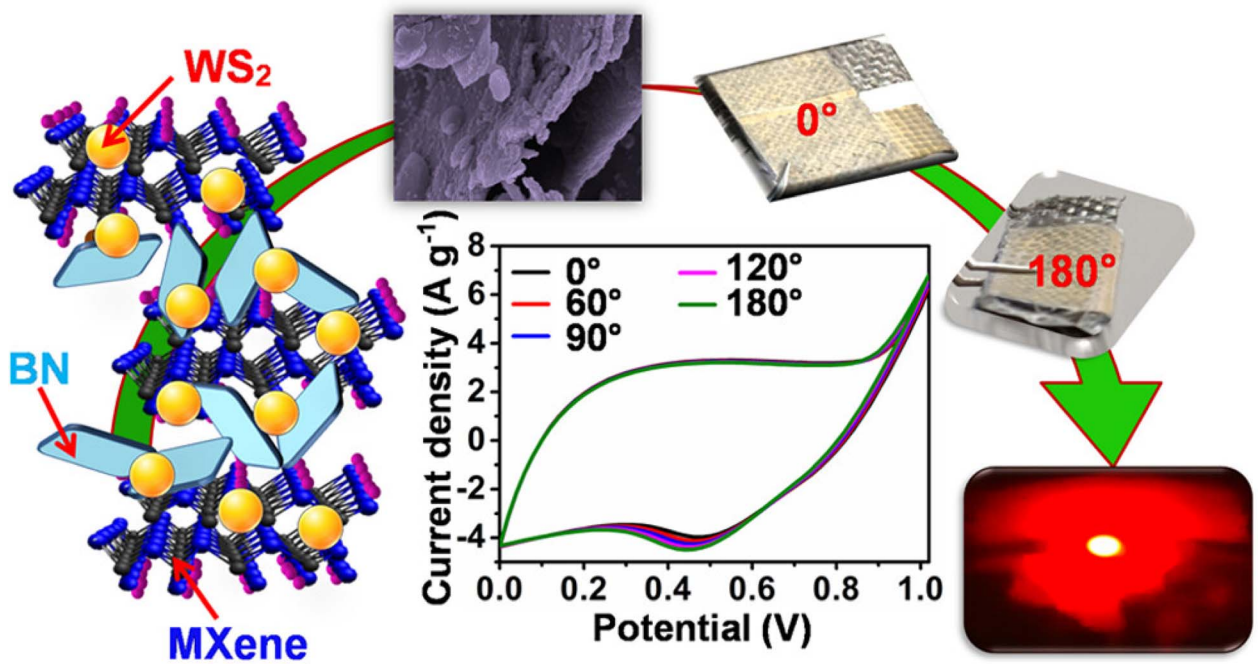

Fig. 5 WS_2/boron nitride/$Ti_3C_2T_x$ MXene binary composite nanostructure for supercapacitor applications, adapted/reproduced from ref. 75 with permission from the American Chemical Society, Copyright 2023.

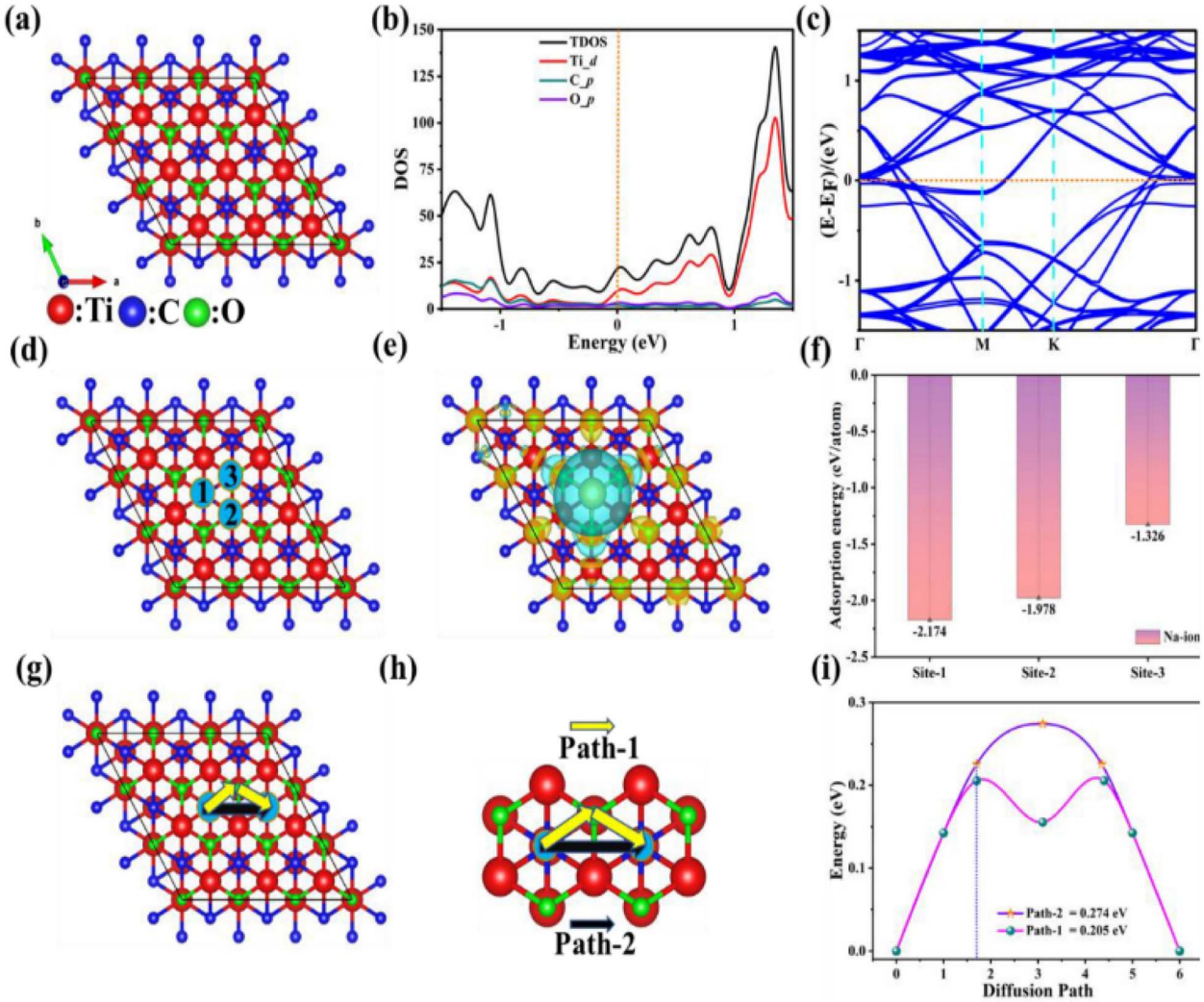

Fig. 6 (a–c) Optimized crystal structure, density of states and band structure of $Ti_3C_2T_x$ (T_x = O). (d) Crystal structure with suitable adsorption sites. (e and f) Charge density difference and adsorption energy of Na^+ ion on the surface of $Ti_3C_2T_x$. (g–i) Diffusion paths and diffusion energy plots, adapted/reproduced from ref. 76 with permission from Elsevier, Copyright 2024.

$Ti_3C_2T_x$ MXene for energy harvesting

Recently, Shrabani and colleagues reported the synthesis of a WS_2-covered $Ti_3C_2T_x$ MXene/boron nitride (BN) composite for supercapacitors using the hydrothermal technique at 180 °C for 12 h, as shown in Fig. 5.[75] Here, the multilayered $Ti_3C_2T_x$ MXene was composed of stacked layers of BN and formed homogeneous dispersions of the MBN binary composite. The optimum electrode revealed a high specific capacitance (SC) of 1318 F g^{-1} in 1 M KOH at 1 A g^{-1}, which displayed an excellent cyclic life after 10 000 charge and discharge runs (retaining around 84% of its initial capacitance). The synthesized composite showed specific energy density and capacitance values of 19.5 Wh kg^{-1} and 140 F g^{-1}, respectively, using commercial PVA-KOH-KI gel as the electrolyte. The strong interactions between individual components were the main factor contributing to these excellent results.

To support and interpret the experimental results, Xiaofeng employed first-principles calculations to optimize the band energy, density of states, and crystal structure of $Ti_3C_2T_x$ MXene.[76] As depicted in Fig. 6, the optimized structure of MXene is $Ti_3C_2T_x$ (T_x = O), with the main band structures of p-orbitals originating from C and O atoms, while d-orbitals originate from Ti.[77] These optimized crystal structures indicate that $Ti_3C_2T_x$ possesses higher conductivity, making it suitable for high cyclability and good rate capability. Fig. 6d illustrates the favourable adsorption sites for Na^+ ions based on the charge density difference. This calculation demonstrates that Na^+ ions adsorbed on the surface of MXene lose charges, which contributes to the charge acceptance of the electrode system. The results of the charge density difference reveal that Na^+ ions are favorable for facilitating the flexible loss of charges in the electrode.

Overall, MXenes exhibit competitive performance relative to graphene and TMDs due to their unique combination of physicochemical properties and hybrid charge-storage mechanisms involving both electric double-layer capacitance and

Table 4 Comparison of $Ti_3C_2T_x$ MXenes, graphene, and transition metal dichalcogenides (TMDs) as electrode materials for supercapacitors[78]

Property	$Ti_3C_2T_x$ MXenes	Graphene	TMDs (MoS_2)
Charge storage mechanism	Hybrid EDLC and pseudocapacitance	Primarily EDLC	Predominantly pseudocapacitance and ion intercalation
Gravimetric capacitance	400–1500 F g^{-1}	100–550 F g^{-1}	100–400 F g^{-1}
Volumetric capacitance	Up to 1500 F cm^{-3}	Up to 550 F cm^{-3}	Typically, lower than MXenes
Electrolyte accessibility	Interlayer ion transport	Surface-limited	Limited by slow intercalation kinetics

pseudocapacitance (Table 4).[78] Among these materials, graphene currently offers advantages in terms of cost and long-term stability, making it more suitable for near-term commercial applications. At the laboratory scale, the production cost of MXenes is estimated to be approximately USD 20.33 per gram in 2024,[79] indicating that further cost reduction is required before their large-scale commercialization. In contrast, the global graphite market is projected to expand from USD 8.32 billion in 2025 to USD 13.35 billion by 2032.[80] Nevertheless, the MXene market is expected to reach approximately USD 121.5 million by 2027,[81] reflecting growing industrial interest and the potential for MXenes to emerge as a competitive class of materials once scalable and cost-effective synthesis strategies are fully matured.

$Ti_3C_2T_x$ MXenes for gas sensors

In 2023, Seyed and colleagues reported the excellent gas sensing performance of $Ti_3C_2T_x$ MXenes and their composites with PDS-Cl conjugated polymers.[82] The strong electrostatic interactions between $Ti_3C_2T_x$ MXenes and polymers formed several heterojunction interfaces *via* hydrogen bonding and ion–dipole interactions, which are beneficial for gas-sensing activities. In particular, the optimized composite displayed the highest sensing signal of around 2% upon exposure to 5 ppm of H_2S gas in comparison to pure $Ti_3C_2T_x$ MXene, as shown in Fig. 7. Moreover, the noise level in the optimal composite was higher than that in the pure $Ti_3C_2T_x$ MXene, which is attributed to the fact that the polymer modifies the charge transport between each layer.

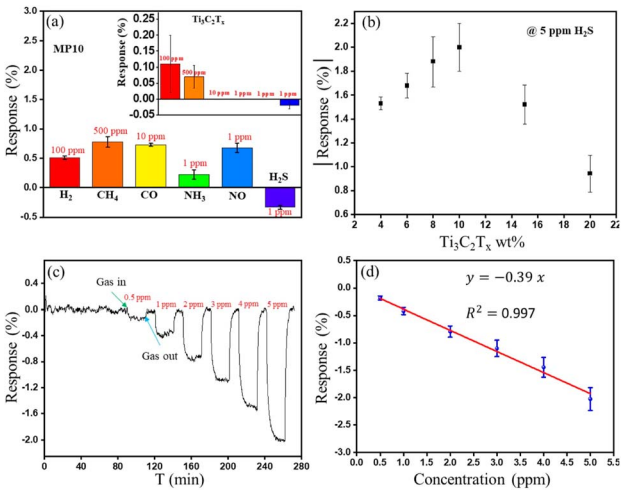

Fig. 7 (a–d) H_2S sensing response values of $Ti_3C_2T_x$ MXene and $Ti_3C_2T_x$ MXene-organic heterostructure (the inset presents the gas selectivity of pure MXene), adapted/reproduced from ref. 82 with permission from the American Chemical Society, Copyright 2023.

Moreover, Ta *et al.* reported the most stable configuration of a $Ti_3C_2T_x/MoS_2$ sensor composite through density functional theory calculation using the Vienna *Ab initio* Simulation Package, as shown in Fig. 8. $Ti_3C_2T_x$ (T_x = OH) and $Ti_3C_2T_x$ (T_x = F) are less stable than $Ti_3C_2T_x$ (T_x = O) according to the DFT calculations of the $Ti_3C_2T_x$ MXene surfaces.[83] In particular, the stability of these configurations differs depending on the types of gas molecules. The adsorption of NO_2 molecules on the composite surface was estimated to be stronger than that of CH_4 or CO_2, which explains the good sensing performance of the composite toward NO_2 molecules (response 40%; 20 ppm of NO_2). Specifically, the stronger adsorption of NO_2 compared to CO_2 and CH_4 originates from the formation of strong interactions at the composite interface, which are absent or significantly weaker for other gases. These interactions promote pronounced charge redistribution at the MoS_2 surface, leading to a larger modulation of the electronic structure and consequently a stronger sensing response. In general, beyond identifying adsorption configurations with weak or strong interactions, DFT analysis elucidates the binding mechanisms between the target gas molecules and the composite surface, distinguishing between physisorption and chemisorption. Gas selectivity is predicted by comparing adsorption energy values, the formation of localized active adsorption sites, and the density of states near the Fermi level of the sensor composites. These insights provide fundamental guidance for rational material design and the selection of suitable sensing gases.

$Ti_3C_2T_x$ MXenes for photo-electrochemical water splitting and triboelectric nanogenerator

Adem *et al.*[85] prepared a novel binary $Ti_3C_2T_x/WO_3/ZnO$ composite using post-annealing procedures and radio frequency sputtering and studied its photoelectrochemical (PEC) performance under solar light irradiation, demonstrating superior photoconversion efficiency. According to the results, at +0.4 V *vs.* RHE in 0.1 M KOH electrolyte, the optimal $Ti_3C_2T_x/$

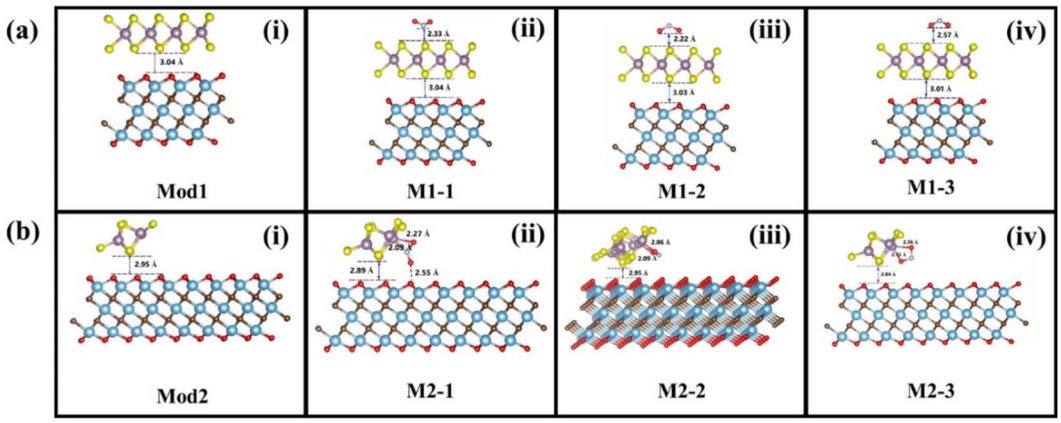

Fig. 8 (a_{i-iv}) Optimized structures and (b_{i-iv}) stable configurations of the as-prepared $Ti_3C_2T_x/MoS_2$ sensor composite when exposed to NO_2 molecules, adapted/reproduced from ref. 84 with permission from Elsevier, Copyright 2022.

WO_3/ZnO binary heterostructure enhanced the photocurrent generation (1.4×10^{-3} A cm^{-2}) in comparison with pristine ZnO (7.8×10^{-4} A cm^{-2}) and the WO_3/ZnO composite (1.1×10^{-3} A cm^{-2}). As shown in Fig. 9, the superior PEC performance achieved by the $Ti_3C_2T_x/WO_3$/ZnO binary composite can be explained by the formation of a Schottky barrier and its high charge-carrier separation efficiency.[85]

Recently, Shaochun *et al.* reported that the strength of the $Ti_3C_2T_x$ MXene/substrate interface substantially affects the electrical and mechanical properties of $Ti_3C_2T_x$ MXene films (Fig. 10). First, the $Ti_3C_2T_x$ MXene was covered on a leather substrate, and then, polyimide (PI) with a thickness of 100 μm was deposited as the electrode *via* laser technology.[86] Finally, a flexible triboelectric tactile sensor was obtained after forming an Au circuit in $HAuCl_4$ solution (5 mg in 1 mL). Interestingly, the as-prepared MXene film displayed good activity in the TENG with the highest output voltage and output power density of 199.56 V and 0.469 mW cm^{-2}, respectively. During the application of external force during movement, charges were generated and induced on PI owing to the different electron affinities. The electrons in the negatively charged $Ti_3C_2T_x$ MXene move to the load when the force is released owing to the edge electric-field leakage effect.[87] This process is gradually repeated in two friction layers and continuously releases electrons to the load, resulting in an alternating voltage. The flexible robust $Ti_3C_2T_x$ MXene/leather films showed excellent cycling performance with long-time operation (more than 1 hour), which can be used in smart wearable and health monitoring devices.[88,89]

In general, the design of MXene-based catalysts for overall energy harvesting has mainly focused on heterostructure engineering, alloying, and electronic structure optimization at the

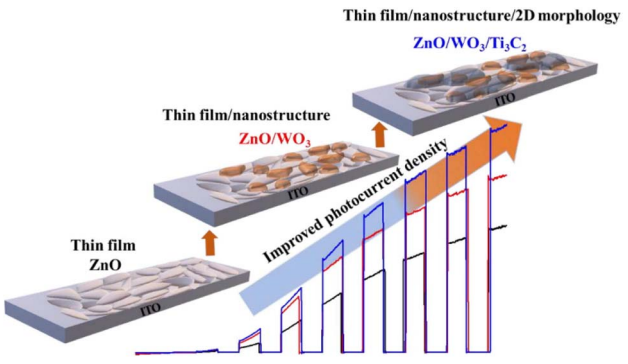

Fig. 9 ZnO/WO_3 composites interfaced with metallic $Ti_3C_2T_x$ MXene for enhanced photoelectrochemical water splitting, adapted/reproduced from ref. 85 with permission from Elsevier, Copyright 2023.

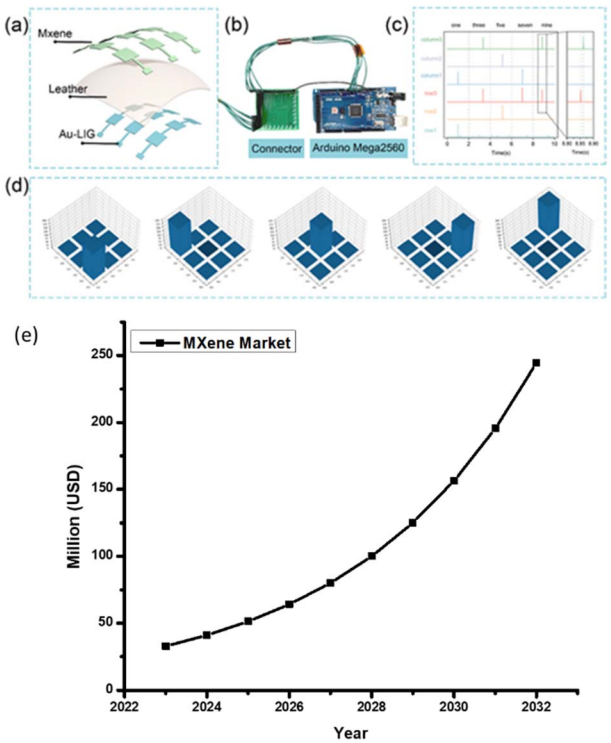

Fig. 10 (a–d) Schematic of a flexible TENG based on a robust $Ti_3C_2T_x$ MXene/leather PI film for human-machine movement, adapted/reproduced from ref. 86 with permission from the American Chemical Society, Copyright 2023. (e) Global MXene market forecast to 2033 (adapted from the MXene Market Insights research report https://www.24chemicalresearch.com/reports/283167/global-mxene-market).

Table 5 Representative $Ti_3C_2T_x$ MXene-based composites for photocatalysis and water remediation

Catalysts	Pollutants	Reaction time	Proposed mechanism	Efficiency	Ref.
$Ti_3C_2T_x$	Ciprofloxacin (10 ppm)	20 min	Adsorption/electrochemical regeneration	208.2 mg g^{-1}	94
$Al_2O_3/Ti_3C_2T_x$	Rhodamine B (15 ppm)	60 min	Adsorption	99.8%	95
	Methylene blue (15 ppm)	60 min		99.9%	
$Bi_4Ti_3O_{12}/Ti_3C_2T_x$	Rhodamine B (5 ppm)	50 min	Photocatalytic degradation	100%	96
	Methyl orange (5 ppm)	50 min		100%	
$Fe/C/Ti_3C_2T_x$	Methylene blue (4000 ppm)	30 min	Photocatalytic degradation	81.2%	97
$CuNiAl/Ti_3C_2T_x$	Tetracycline (20 ppm)	80 min	Photocatalytic degradation	90.3%	98

laboratory scale. However, studies addressing the influence of the electric double layer at the catalyst–electrolyte interface and ion transfer across different components in composite catalysts remain limited. A deeper understanding of these interfacial processes is essential for achieving performance breakthroughs and enabling large-scale applications. In fact, current techniques still face substantial challenges that hinder practical scale-up. In detail, hydrogen storage during water-splitting processes often relies on ultra-low-temperature tanks, which are costly and energy-intensive. In addition, freeze-drying procedures commonly used for MXene processing are time-consuming, and the high batch-scale production cost of MXenes remains a critical concern. Furthermore, MXene powders used in photo- and electrocatalytic applications must typically be redispersed into colloidal solutions, where oxidation and stability issues arise. The use of organic solvents further complicates storage and necessitates post-treatment and waste-liquid recovery. It is anticipated that with continued technological advancements, these challenges can be gradually addressed, enabling MXene-based water-splitting systems to reach pilot-scale operation by 2050.

$Ti_3C_2T_x$ MXenes for photocatalysis and water remediation

Industry-released wastewater commonly contains a wide range of toxic contaminants, including pesticides, organic dyes, pharmaceuticals, and other harmful aqueous pollutants. $Ti_3C_2T_x$ MXenes have been widely recognized as promising materials for photocatalysis and water remediation due to their outstanding physicochemical properties, such as high adsorption capacity, unique layered structure, and abundant surface functional groups. In water treatment systems, $Ti_3C_2T_x$ MXenes play a crucial role as membrane materials, adsorbents, and catalytic supports. For example, the multilayered $Ti_3C_2T_x$ MXene structure, featuring interlayer channels of approximately 6 Å, enables the efficient removal of organic contaminants.[90] Several studies have reported the development of MXene-based membranes for methylene blue removal, achieving exceptionally high adsorption capacities of up to 28 403.7 mg g^{-1}.[91] Furthermore, reinforcement with cellulose nanofibers effectively suppresses membrane swelling, thereby enhancing structural stability and enabling the efficient removal of antibiotics such as tetracycline, azithromycin, and penicillin G potassium salt.[92]

In addition to adsorption-based remediation, MXenes exhibit an excellent photocatalytic degradation performance under light irradiation. Zeng and co-workers demonstrated the highly efficient degradation of Congo red (98%) and tetracycline hydrochloride (86%) using hierarchical g-$C_3N_4/Ti_3C_2T_x$/polyethersulfone composites.[93] The enhanced degradation efficiency was primarily attributed to the improved light-harvesting capability and the effective suppression of electron–hole recombination achieved through optimized interfacial coupling between g-C_3N_4 and MXene/polyethersulfone.[93] Overall, water remediation *via* adsorption and photo-induced radical pathways using $Ti_3C_2T_x$ MXenes and their composites has shown significant progress recently, which is systematically summarized in Table 5.

Conclusions

In this review, we have basically examined the synthesis strategies and multifunctional applications of $Ti_3C_2T_x$ MXenes across energy, environmental, biomedical, and sensing-related fields. Fluoride-based etching approaches generally enable the production of $Ti_3C_2T_x$ MXenes with relatively large lateral flake sizes and preserved mechanical integrity, which are advantageous for flexible electrodes and structural composites. In contrast, fluoride salt-based and HF aqueous etching methods typically yield smaller flakes and richer surface terminations, which can enhance electrochemical activity but often compromise oxidation stability and long-term durability. These synthesis-dependent trade-offs underscore the necessity of tailoring $Ti_3C_2T_x$ MXene preparation routes to specific application requirements rather than pursuing a general fabrication strategy.

Since the initial discovery of $Ti_3C_2T_x$ MXenes, substantial progress has been achieved in both synthesis control and composite design, establishing $Ti_3C_2T_x$ MXenes as a versatile two-dimensional platform. Nevertheless, several fundamental challenges remain. In particular, oxidation instability under humid or ambient conditions, limited control over surface terminations, batch-to-batch reproducibility, and safety and sustainability concerns associated with fluorine-containing etchants continue to restrict reliable performance and large-scale deployment. Addressing these issues requires a deeper mechanistic understanding of surface chemistry, defect evolution, and interfacial and financial processes under realistic

operating environments. According to the MXene Materials Market Insights report, the global MXene market is projected to reach approximately USD 244.38 million by 2032, corresponding to a compound annual growth rate of 22.7% (Fig. 10e).

From an application perspective, $Ti_3C_2T_x$ MXenes have demonstrated notable potential in biomedical regeneration, energy harvesting, and environmental remediation, especially where high electrical conductivity and surface reactivity are critical. The translation of laboratory-scale demonstrations into practical technologies remains constrained by energy-intensive processing steps, high production costs, and stability challenges during storage and device integration. In this context, emerging strategies such as fluoride-free or green synthesis, secondary $Ti_3C_2T_x$ MXene production from recycled precursors, and machine learning-assisted modelling to optimize synthesis and composite architectures represent promising pathways toward more sustainable and scalable manufacturing.

Controlling product development through stepwise phases of technological advancement remains both an opportunity and a challenge for MXene-based technologies, and this systematic progression has not yet been extensively explored. In terms of technological readiness level (TRL), current MXene research is generally considered to be at TRL 1–2, with some studies approaching TRL 3–4, as no commercially available devices or large-scale applications based on MXenes have yet reached the market. Therefore, replacing conventional materials or integrating MXenes into existing systems represents an important step toward advancing their technological maturity. Achieving higher TRLs will require systematic prototyping and comprehensive evaluation of complete systems or components to demonstrate clear advantages over state-of-the-art commercial materials. Furthermore, establishing clearer commercialization pathways will depend on coordinated progress in synthesis strategies, surface termination control, structural and electronic property optimization, and application-specific performance, which together form the foundation for further advancement of MXene technologies along the TRL scale.[32]

Looking forward, meaningful progress toward commercialization will depend on coordinated advances in synthesis standardization, lifecycle assessments, and device-level validation rather than incremental performance improvements alone. Currently, $Ti_3C_2T_x$ MXenes are unlikely to fully replace traditional materials such as graphene; continued improvements in stability, cost-efficiency, and reproducibility could enable their adoption in high-value applications in energy harvesting and environmental protection (reducing the carbon footprint) within the next one to two decades. Overall, this review highlights both the opportunities and the limitations of $Ti_3C_2T_x$ MXenes and provides a fundamental framework for future research aimed at advancing MXene-based technologies toward reliable, sustainable, and application-ready systems.

Author contributions

Ly Tan Nhiem: figure organization, manuscript preparation.

Conflicts of interest

There are no conflicts to declare.

Data availability

No primary research results, software or code have been included, and no new data were generated or analysed as part of this review.

Supplementary information (SI) is available. See DOI: https://doi.org/10.1039/d5ra08486e.

Acknowledgements

The author would like to thank Ho Chi Minh City University of Technology and Engineering for its support.

References

1 T. K. Pardhi, V. Balaji, S. Sunil, G. Arumugam, V. Naveen, P. Porkodi, A. J. Kottiyatil, K. Madhavan and P. Ghosh, *Sci. Cult.*, 2025, **91**, 37–48.
2 E. Pavón, R. Martín-Rodríguez, A. C. Perdigón and M. D. Alba, *Inorganics*, 2021, **9**, 43.
3 N. Veeramani, M. K. Chaithra, G. Santhana Krishnan, Kalavati and N. T. Manikandanath, *Polym. Eng. Sci.*, 2025, **66**, 1091–1098.
4 D. S. Nakonieczny, G. S. Martynková, M. Hundáková, G. Kratošová, S. Holešová, J. Kupková, L. Pazourková and J. Majewska, *Materials*, 2022, **15**, 1390.
5 V. Naveen, A. P. Deshpande and S. Raja, *RSC Adv.*, 2020, **10**, 33178–33188.
6 M. Naguib, O. Mashtalir, J. Carle, V. Presser, J. Lu, L. Hultman, Y. Gogotsi and M. W. Barsoum, *ACS Nano*, 2012, **6**, 1322–1331.
7 X.-F. Yu, Y.-C. Li, J.-B. Cheng, Z.-B. Liu, Q.-Z. Li, W.-Z. Li, X. Yang and B. Xiao, *ACS Appl. Mater. Interfaces*, 2015, **7**, 13707–13713.
8 W. Bai, L. Shi, Z. Li, D. Liu, Y. Liang, B. Han, J. Qi and Y. Li, *Mater. Today Energy*, 2024, **41**, 101547.
9 S. Vallem, S. Venkateswarlu, S. Song, J. Kim, Y. Li and J. Bae, *Coord. Chem. Rev.*, 2024, **510**, 215778.
10 M. Ghidiu, M. R. Lukatskaya, M. Q. Zhao, Y. Gogotsi and M. W. Barsoum, *MXenes: from Discovery to Applications of Two-Dimensional Metal Carbides and Nitrides*, 2023, pp. 379–399.
11 X. Li, Y. Bai, X. Shi, N. Su, G. Nie, R. Zhang, H. Nie and L. Ye, *Mater. Adv.*, 2021, **2**, 1570–1594.
12 L. Verger, V. Natu, M. Carey and M. W. Barsoum, *Trends Chem.*, 2019, **1**, 656–669.
13 V. T. T. Linh, N. P. T. Trieu, Q. T. H. Ta, N. N. Tri, V. N. Huynh, D. T. Y. Oanh, N. H. Hieu and S. M. Seo, *Vietnam J. Chem.*, 2026, **1**, DOI: 10.1002/vjch.70129.
14 G. Deysher, C. E. Shuck, K. Hantanasirisakul, N. C. Frey, A. C. Foucher, K. Maleski, A. Sarycheva, V. B. Shenoy, E. A. Stach, B. Anasori and Y. Gogotsi, *ACS Nano*, 2020, **14**, 204–217.

15 M. A. Zaed, K. H. Tan, R. Saidur, N. Abdullah and A. K. Pandey, *J. Mater. Sci.*, 2024, **59**, 7575–7594.
16 N. M. Tran, Q. T. H. Ta, A. Sreedhar and J.-S. Noh, *Appl. Surf. Sci.*, 2021, **537**, 148006.
17 Y. Fan, Z. Yuan, G. Zou, Q. Zhang, B. Liu and Q. Peng, *Catal. Today*, 2018, **318**, 167–174.
18 X. Zhao, A. Vashisth, E. Prehn, W. Sun, S. A. Shah, T. Habib, Y. Chen, Z. Tan, J. L. Lutkenhaus, M. Radovic and M. J. Green, *Matter*, 2019, **1**, 513–526.
19 W. Y. Chen, S.-N. Lai, C.-C. Yen, X. Jiang, D. Peroulis and L. A. Stanciu, *ACS Nano*, 2020, **14**, 11490–11501.
20 W. Cao, J. Nie, Y. Cao, C. Gao, M. Wang, W. Wang, X. Lu, X. Ma and P. Zhong, *Chem. Eng. J.*, 2024, **496**, 154097.
21 A. Sreedhar, P. Ravi and J.-S. Noh, *J. Mater. Sci. Technol.*, 2024, **203**, 237–254.
22 M. A. Zaed, J. Paul, S. Aktar, J. Jacob, K. H. Tan and P. Thomas, *Energy Nexus*, 2026, **21**, 100625.
23 P. Kuang, J. Low, B. Cheng, J. Yu and J. Fan, *J. Mater. Sci. Technol.*, 2020, **56**, 18–44.
24 S. Myhra, J. A. A. Crossley and M. W. Barsoum, *J. Phys. Chem. Solids*, 2001, **62**, 811–817.
25 M. Naguib, M. Kurtoglu, V. Presser, J. Lu, J. Niu, M. Heon, L. Hultman, Y. Gogotsi and M. W. Barsoum, *Adv. Mater.*, 2011, **23**, 4248–4253.
26 L. Yang, D. Kan, C. Dall'Agnese, Y. Dall'Agnese, B. Wang, A. K. Jena, Y. Wei, G. Chen, X. F. Wang, Y. Gogotsi and T. Miyasaka, *J. Mater. Chem. A*, 2021, **9**, 5016–5025.
27 P. Das and Pooja, *Hazardous Gases: Risk Assessment on the Environment and Human Health*, 2021, pp. 153–167.
28 D. Masekela, P. J. Mafa, T. L. Yusuf, S. A. Balogun, A. T. Kuvarega and K. D. Modibane, *Coord. Chem. Rev.*, 2026, **549**, 217270.
29 A. Mashele, N. S. Seroka and L. Khotseng, *Renewable Sustainable Energy Rev.*, 2026, **226**, 116373.
30 A. Iqbal, T. Hassan, S. M. Naqvi, Y. Gogotsi and C. M. Koo, *Nat. Rev. Electr. Eng.*, 2024, **1**, 180–198.
31 M. Downes, C. E. Shuck, B. McBride, J. Busa and Y. Gogotsi, *Nat. Protoc.*, 2024, **19**, 1807–1834.
32 C. E. Shuck, A. Sarycheva, M. Anayee, A. Levitt, Y. Zhu, S. Uzun, V. Balitskiy, V. Zahorodna, O. Gogotsi and Y. Gogotsi, *Adv. Eng. Mater.*, 2020, **22**, 1901241.
33 A. Lipatov, M. Alhabeb, M. R. Lukatskaya, A. Boson, Y. Gogotsi and A. Sinitskii, *Adv. Electron. Mater.*, 2016, **2**, 1600255.
34 C. J. Zhang, S. Pinilla, N. McEvoy, C. P. Cullen, B. Anasori, E. Long, S. H. Park, A. Seral-Ascaso, A. Shmeliov, D. Krishnan, C. Morant, X. Liu, G. S. Duesberg, Y. Gogotsi and V. Nicolosi, *Chem. Mater.*, 2017, **29**, 4848–4856.
35 M. Alhabeb, K. Maleski, B. Anasori, P. Lelyukh, L. Clark, S. Sin and Y. Gogotsi, *Chem. Mater.*, 2017, **29**, 7633–7644.
36 A. Jawaid, A. Hassan, G. Neher, D. Nepal, R. Pachter, W. J. Kennedy, S. Ramakrishnan and R. A. Vaia, *ACS Nano*, 2021, **15**, 2771–2777.
37 N. Kumar, Q. V. Hoang, B. Mohammad, K. R. Kaja, P. H. Nguyen, Q. L. Van, V. Vien, V. T. T. Linh, P. K. T. Nguyen and Q. T. H. Ta, *J. Sci.:Adv. Mater. Devices*, 2025, **4**, 101034.
38 A. Lipatov, A. Goad, M. J. Loes, N. S. Vorobeva, J. Abourahma, Y. Gogotsi and A. Sinitskii, *Matter*, 2021, **4**, 1413–1427.
39 Q. Xue, H. Zhang, M. Zhu, Z. Pei, H. Li, Z. Wang, Y. Huang, Y. Huang, Q. Deng, J. Zhou, S. Du, Q. Huang and C. Zhi, *Adv. Mater.*, 2017, **29**, 1604847.
40 J. Zhang, N. Kong, S. Uzun, A. Levitt, S. Seyedin, P. A. Lynch, S. Qin, M. Han, W. Yang, J. Liu, X. Wang, Y. Gogotsi and J. M. Razal, *Adv. Mater.*, 2020, **32**, 2001093.
41 C. Zhang, B. Anasori, A. Seral-Ascaso, S.-H. Park, N. McEvoy, A. Shmeliov, G. S. Duesberg, J. N. Coleman, Y. Gogotsi and V. Nicolosi, *Adv. Mater.*, 2017, **29**, 1702678.
42 M. W. Barsoum and Y. Gogotsi, *Ceram. Int.*, 2023, **49**, 24112–24122.
43 V. Natu, M. Sokol, L. Verger and M. W. Barsoum, *J. Phys. Chem. C*, 2018, **122**, 27745–27753.
44 Z. Khalid, F. Hadi, J. Xie, V. Chandrabose and J.-M. Oh, *Small*, 2025, **21**, 2407856.
45 Z. Cai and H. Kim, *npj 2D Mater. Appl.*, 2025, **9**, 66.
46 K. K. Swain, S. K. Pradhan and D. J. Late, *ChemistrySelect*, 2025, **10**, e202404885.
47 S. Lee, E. Yang, J. Lee, T. Y. Ko and S. J. Kim, *Adv. Mater.*, 2025, **37**, 2502440.
48 G. Bhuvaneshwari, N. Ponpandian and C. Viswanathan, *Surf. Interfaces*, 2025, **67**, 106583.
49 M. Y. Bhat, W. A. Adeosun, K. Prenger, Y. A. Samad, K. Liao, M. Naguib, S. Mao and A. Qurashi, *Adv. Compos. Hybrid Mater.*, 2024, **8**, 52.
50 C. I. Idumah, *Polym.-Plast. Technol. Mater.*, 2023, **62**, 443–466.
51 M. Safarkhani, B. F. Far, Y. S. Huh and N. Rabiee, *ACS Biomater. Sci. Eng.*, 2023, **9**, 6516–6530.
52 C. Qiao, H. Wu, X. Xu, Z. Guan and W. Ou-Yang, *Adv. Mater. Interfaces*, 2021, **8**, 2100903.
53 C. J. Zhang, M. P. Kremer, A. Seral-Ascaso, S.-H. Park, N. McEvoy, B. Anasori, Y. Gogotsi and V. Nicolosi, *Adv. Funct. Mater.*, 2018, **28**, 1705506.
54 M. Dadashi Firouzjaei, S. K. Nemani, M. Sadrzadeh, E. K. Wujcik, M. Elliott and B. Anasori, *Adv. Mater.*, 2023, **35**, 2300422.
55 S. Jolly, M. P. Paranthaman and M. Naguib, *Mater. Today Adv.*, 2021, **10**, 100139.
56 Y. Zhong, S. Huang, Z. Feng, Y. Fu and A. Mo, *J. Biomed. Mater. Res., Part A*, 2022, **110**, 1840–1859.
57 D. Ayodhya, *Diamond Relat. Mater.*, 2023, **132**, 109634.
58 G. Perini, A. Rosenkranz, G. Friggeri, D. Zambrano, E. Rosa, A. Augello, V. Palmieri, M. De Spirito and M. Papi, *Biomed. Pharmacother.*, 2022, **153**, 113496.
59 G. Yang, F. Liu, J. Zhao, L. Fu, Y. Gu, L. Qu, C. Zhu, J.-J. Zhu and Y. Lin, *Coord. Chem. Rev.*, 2023, **479**, 215002.
60 S. Iravani and R. S. Varma, *Nano-Micro Lett.*, 2022, **14**, 213.
61 S. Iravani, E. Nazarzadeh Zare and P. Makvandi, *ACS Biomater. Sci. Eng.*, 2024, **10**, 1892–1909.
62 X. Qu, Y. Guo, C. Xie, S. Li, Z. Liu and B. Lei, *ACS Nano*, 2023, **17**, 7229–7240.
63 Y. Wei, P. Zhang, R. A. Soomro, Q. Zhu and B. Xu, *Adv. Mater.*, 2021, **33**, 2103148.

64 B. Lu, Z. Zhu, B. Ma, W. Wang, R. Zhu and J. Zhang, *Small*, 2021, **17**, 2100946.
65 R. Deng, M. Chang, Y. Chen and Y. Zhou, *Nanophotonics*, 2022, **11**, 4995–5017.
66 B. Xu and Y. Gogotsi, *Adv. Funct. Mater.*, 2020, **30**, 47.
67 Z. Gao, W. Feng, M. Zhang, S. Xu, J. Zhang, J. Jiang, J. Li, B. Li, L. Xie and W. Zhao, *Appl. Mater. Today*, 2025, **47**, 102949.
68 L. Mao, S. Hu, Y. Gao, L. Wang, W. Zhao, L. Fu, H. Cheng, L. Xia, S. Xie, W. Ye, Z. Shi and G. Yang, *Adv. Healthcare Mater.*, 2020, **9**, 2000872.
69 C.-Y. Lee, Y.-T. Hsu, Q.-C. Huang, P. Subramaniyan, A. K. Paulose, C.-C. Huang and T.-E. Lin, *Small*, 2025, **22**, e08633.
70 X. Wang, Y. Sang, H. Zhang, B. Zheng, B. Wang, Y. Hu and R. Wu, *Int. J. Biol. Macromol.*, 2026, **339**, 149645.
71 K. Diedkova, A. D. Pogrebnjak, S. Kyrylenko, K. Smyrnova, V. V. Buranich, P. Horodek, P. Zukowski, T. N. Koltunowicz, P. Galaszkiewicz, K. Makashina, V. Bondariev, M. Sahul, M. Caplovicova, Y. Husak, W. Simka, V. Korniienko, A. Stolarczyk, A. Blacha-Grzechnik, V. Balitskyi, V. Zahorodna, I. Baginskiy, U. Riekstina, O. Gogotsi, Y. Gogotsi and M. Pogorielov, *ACS Appl. Mater. Interfaces*, 2023, **15**, 14033–14047.
72 C. Liang, F. Ai, P. Wang, J. kang, H. Deng, Z. Fan, Z. Lin, G. Liu, Y. Zhu and J. Tao, *Int. J. Biol. Macromol.*, 2026, **335**, 149207.
73 K. Chen, Y. Chen, Q. Deng, S. H. Jeong, T. S. Jang, S. Du, H. E. Kim, Q. Huang and C. M. Han, *Mater. Lett.*, 2018, **229**, 114–117.
74 S. H. Lee, S. Jeon, X. Qu, M. S. Kang, J. H. Lee, D. W. Han and S. W. Hong, *Nano Convergence*, 2022, **9**, 38.
75 S. De, S. Acharya, C. K. Maity and G. C. Nayak, *ACS Appl. Nano Mater.*, 2023, **6**, 11175–11186.
76 X. Zhang, M. S. Javed, H. Ren, X. Zhang, S. Ali, K. Han, A. Ahmad, A. M. Tighezza, W. Han and K.-Q. Peng, *Mater. Today Energy*, 2024, **40**, 101496.
77 X. Zhang, M. S. Javed, S. Ali, A. Ahmad, S. S. A. Shah, I. Hussain, D. Choi, A. M. Tighezza, E. Tag-Eldin and C. Xia, *Nano Energy*, 2024, **120**, 109108.
78 D. B. Tripathy, S. Pradhan, P. Agarwal and D. Jain, *Sustainable Energy Fuels*, 2026, **2**, 447–487.
79 M. A. Zaed, K. H. Tan, N. Abdullah, R. Saidur, A. K. Pandey and A. M. Saleque, *Open Ceram.*, 2024, **17**, 100526.
80 Graphite Market Analysis: Projected to Reach USD 13.35 Billion by 2032 with a CAGR of 6.9% - EIN Presswire, https://www.einnews.com/pr_news/789993641/graphite-market-analysis-projected-to-reach-usd-13-35-billion-by-2032-with-a-cagr-of-6-9, accessed 8 January 2026.
81 MXene Market Size Report, 2022-2027, https://www.industryarc.com/Report/20088/MXene-market.html, accessed 8 January 2026.
82 S. H. Hosseini-Shokouh, J. Zhou, E. Berger, Z.-P. Lv, X. Hong, V. Virtanen, K. Kordas and H.-P. Komsa, *ACS Appl. Mater. Interfaces*, 2023, **15**, 7063–7073.
83 Q. T. H. Ta, A. Sreedhar, N. N. Tri and J.-S. Noh, *Ceram. Int.*, 2024, **50**, 27227–27236.
84 Q. T. H. Ta, N. N. Tri and J.-S. Noh, *Appl. Surf. Sci.*, 2022, **604**, 154624.
85 A. Sreedhar, Q. T. H. Ta and J.-S. Noh, *J. Electroanal. Chem.*, 2023, **940**, 117509.
86 S. Zhang, Y. Xiao, H. Chen, Y. Zhang, H. Liu, C. Qu, H. Shao and Y. Xu, *ACS Appl. Mater. Interfaces*, 2023, **15**, 13802–13812.
87 Y. Liu, Z. Shi, T. Liang, D. Zheng, Z. Yang, Z. Wang, J. Zhou and S. Wang, *InfoMat*, 2024, **6**, e12536.
88 A. Kumar, R. K. R. Kumar, M. O. Shaikh, J.-Y. Yang, A. M. Bharti, B.-Y. Huang, H.-L. Chang, D.-H. Lee and C.-H. Chuang, *Mater. Today Chem.*, 2024, **37**, 102024.
89 P. Wang, T. Mai, W. Zhang, M. Qi, L. Chen, Q. Liu and M. Ma, *Small*, 2024, **20**, 2304914.
90 L. Huang, L. Ding, J. Caro and H. Wang, *Angew. Chem., Int. Ed.*, 2023, **62**, e202311138.
91 C. Yao, W. Zhang, L. Xu, M. Cheng, Y. Su, J. Xue, J. Liu and S. Hou, *Sep. Purif. Technol.*, 2021, **263**, 118365.
92 H. Zhang, Y. Zheng, H. Zhou, S. Zhu and J. Yang, *Sep. Purif. Technol.*, 2023, **305**, 122425.
93 G. Zeng, Z. He, T. Wan, T. Wang, Z. Yang, Y. Liu, Q. Lin, Y. Wang, A. Sengupta and S. Pu, *Sep. Purif. Technol.*, 2022, **292**, 121037.
94 A. A. Ghani, A. Shahzad, M. Moztahida, K. Tahir, H. Jeon, B. Kim and D. S. Lee, *Chem. Eng. J.*, 2021, **421**, 127780.
95 Q. Long, S. Zhao, J. Chen, Z. Zhang, G. Qi and Z. Q. Liu, *J. Membr. Sci.*, 2021, **635**, 119464.
96 Y. Wang, J. Chen, M. Que, Q. Wu, X. Wang, Y. Zhou, Y. Ma, Y. Li and X. Yang, *Appl. Surf. Sci.*, 2023, **639**, 158270.
97 W. Zhang, Q. Zhang, X. Yang, M. Ran, Y. Ding and P. La, *Mater. Sci. Eng., B*, 2026, **325**, 119120.
98 Z. Gao, D. Wang, B. Zou, Y. Liu, X. Yu, Q. Li, J. Ma, L. Liu, C. Liu, Z. Tong and J. Hu, *J. Taiwan Inst. Chem. Eng.*, 2026, **182**, 106584.